Particle Detectors

A brief introduction with emphasis on high energy physics applications

TRIUMF Summer Institute 2006
July 10-21 2006

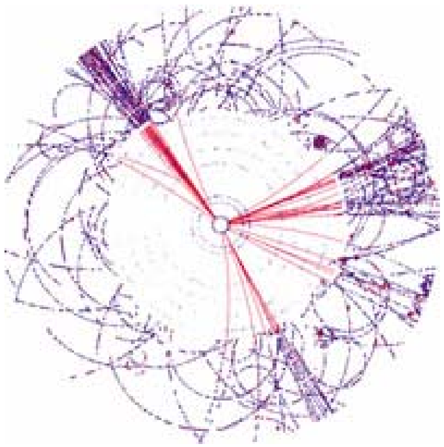

- Lecture I
  - measurement of ionization and position
- Lecture II
  - scintillation and photo detection
  - calorimetry
- Lecture III
  - particle identification
  - detector systems

Michel Lefebvre
Physics and Astronomy
University of Victoria

Literature on particle detectors

- Textbooks
  - C. Grupen, Particle Detectors, Cambridge University Press, 1996.
  - K. Kleinknecht, Detectors for Particle Radiation, Cambridge University Press, 1999
  - G. Knoll, Radiation Detection and Measurement, John Wiley and Sons, third edition, 1999.
  - W.R. Leo, Techniques for Nuclear and Particle Physics Experiments, second revised edition, Springer-Verlag, 1994.
- Review articles and other sources
  - Experimental Techniques in High Energy Physics, T. Ferbel (editor), World Scientific, 1991.
  - Instrumentation in High Energy Physics, F. Sauli (editor), World Scientific, 1992.
  - Annual Review of Nuclear and Particle Science
  - Particle Data Group, Review of Particle Physics, S. Eidelman *et al.*, Phys. Lett. B**592**, 1 (2004)

Lecture I

- Measurement of ionization and position
  - Bethe-Bloch
  - Ionization chambers
  - Silicon detectors
  - Proportional chambers
  - Multi wire proportional chambers
  - Drift chambers
  - Micro gaseous detectors

Interactions of charged particles

- Consider particles heavier than the electron
  - Inelastic collisions with the atomic electrons of the material dominate, but also
    - elastic scattering from nuclei
    - emission of Cherenkov radiation
    - bremsstrahlung
  - soft inelastic collisions
    - excitation
  - hard inelastic collisions
    - ionization
      - e^- possibly causing other ionization: δ-rays, knock-on e^-

Interactions of charged particles

Maximum transfer of kinetic energy

- head-on collision

of an electron →
$$T^{\max} = \frac{2m_e c^2\beta^2\gamma^2}{1+2\gamma b+b^2} \qquad b \equiv \frac{m_e}{m}$$
γ, β, *m, p, E* of incident particle

- low energy $m > m_e$

$$T^{\max} = 2m_e c^2\beta^2\gamma^2 \quad \text{for} \quad \gamma b \ll \tfrac{1}{2}$$

- very high energy $m > m_e$

$$T^{\max} \to E \quad \text{for} \quad \gamma b \gg \tfrac{1}{2}$$

- $m = m_e$

$$T^{\max} = (\gamma - 1)m_e c^2 = E - m_e c^2$$

Energy loss by ionization and excitation

Bethe-Bloch formula

- mean rate of energy loss, or stopping power
  - ionization only + density and shell corrections
  - for moderately relativistic charged particles ($m > m_e$)

$$\left\langle \frac{dE}{dx} \right\rangle = -4\pi N_A r_e^2 m_e c^2 z^2 \frac{Z}{A} \frac{1}{\beta^2} \left[\frac{1}{2} \ln \frac{2 m_e c^2 \beta^2 \gamma^2 T^{\max}}{I^2} - \beta^2 - \frac{\delta}{2} - \frac{C}{Z} \right]$$

  - MeV g^{-1} cm^2 ➔ beware x is (length)×(density)
  - incident particle: z, β, γ, m, $T^{\max}$
  - absorber: Z, A, I, δ, C (atomic shell corrections)

$I \approx 16 Z^{0.9}$ eV for $Z > 1$ ionization constant

$\delta \approx 2 \ln \gamma + \text{constant(material)}$ density effect ➔ Fermi plateau

  - constant: $4\pi N_A r_e^2 m_e c^2 = 0.3071$ MeV $\text{cm}^2 \text{mol}^{-1}$

Energy loss by ionization and excitation

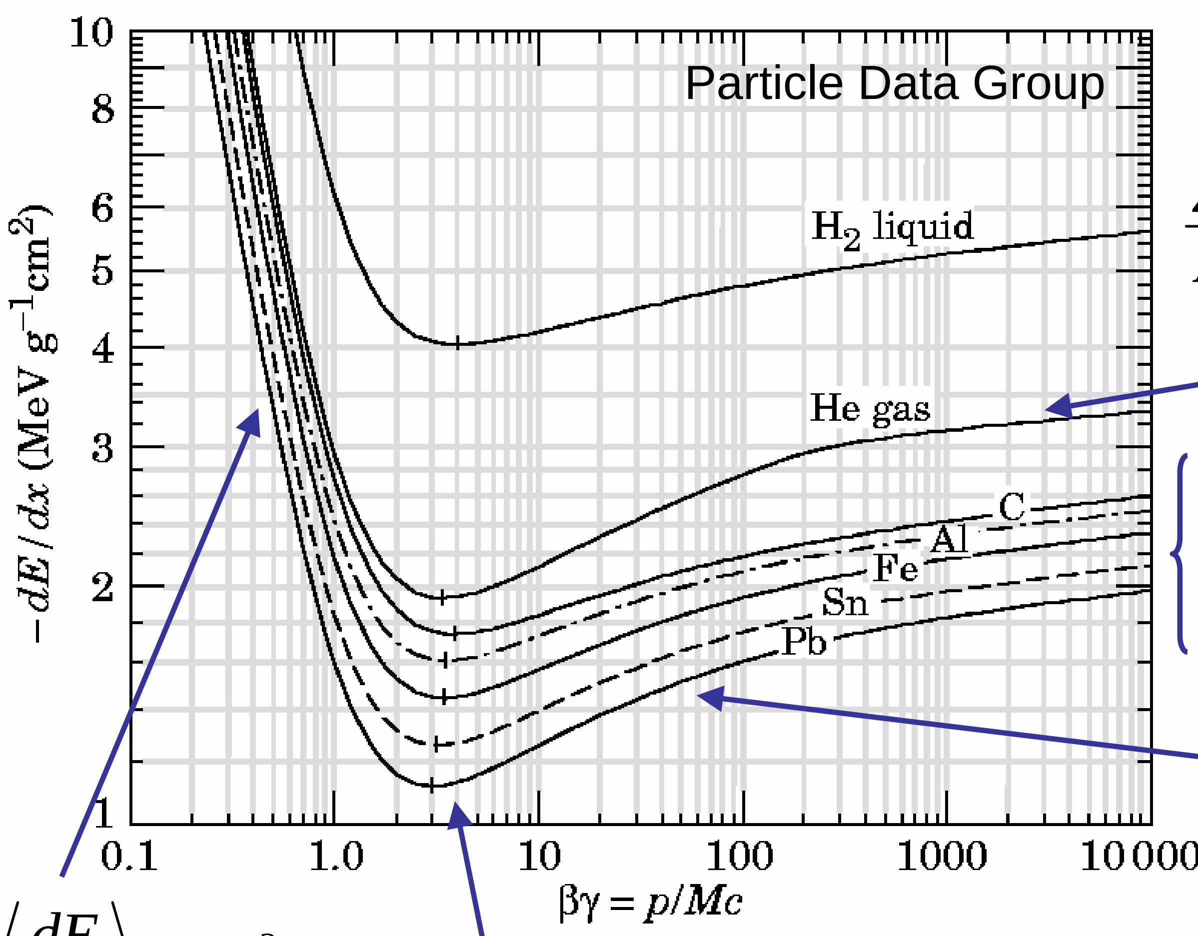

$$\frac{Z}{A} = 1$$

"density effect", "Fermi plateau"

$$\frac{Z}{A} \approx 0.5$$ ~ electron density

$$\left\langle \frac{dE}{dx} \right\rangle \propto \ln \beta^2\gamma^2$$

"relativistic rise"

$$\left\langle \frac{dE}{dx} \right\rangle \propto \beta^{-2}$$

"kinematical term"

$\beta\gamma \approx 3$ to 4

MIP (minimum ionizing particle)

Radiative losses

- Bremsstrahlung important at high energy
  - and for electrons! See Calorimetry.

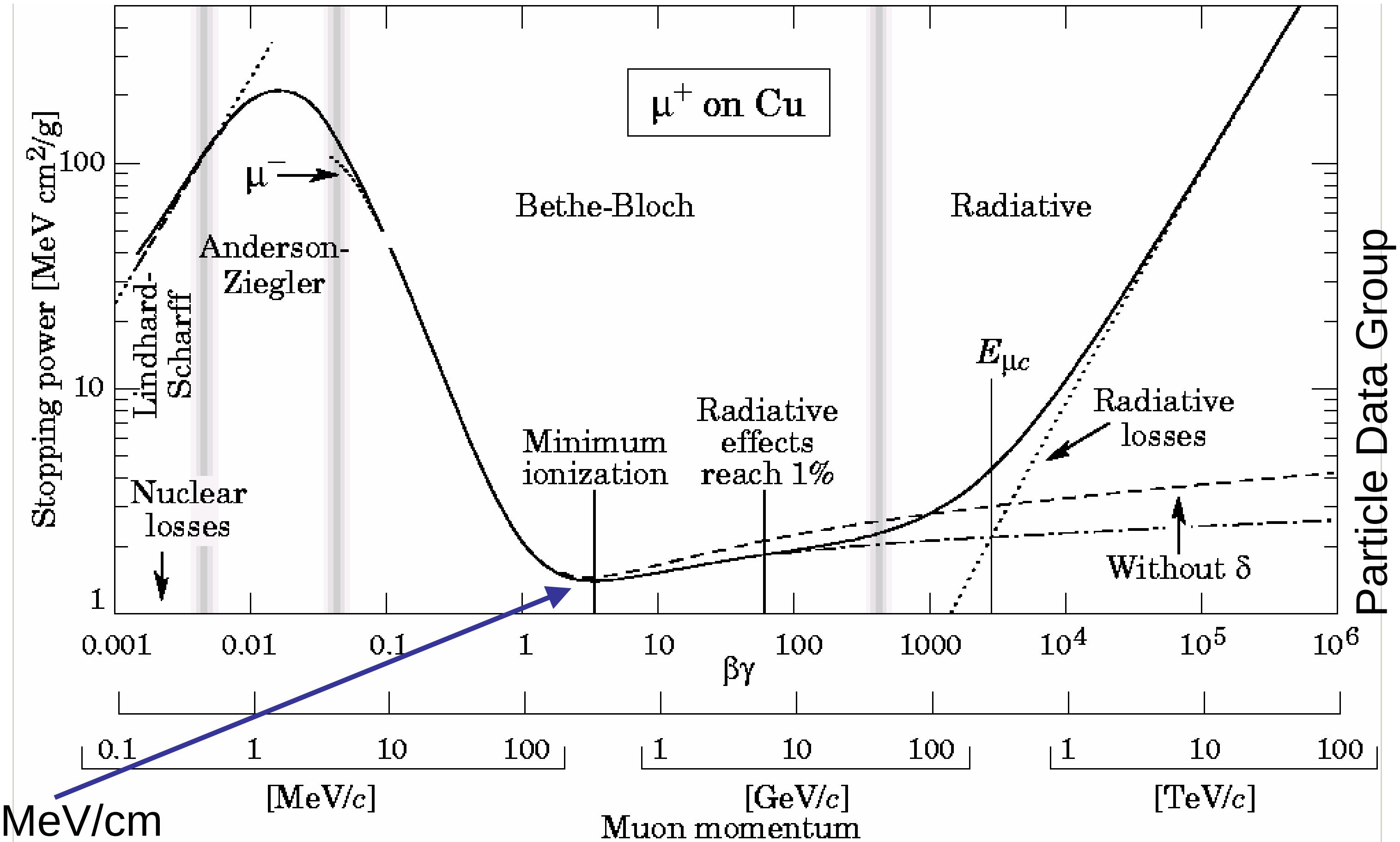

12.90 MeV/cm

Fluctuations in energy loss

- Real detectors have limited granularity
  - measure $\Delta E/\Delta x$
  - thin layers (or low ρ)
    - few collisions, some with high energy transfer
    - “Landau tails”
  - thick layers (or high ρ)
    - many collisions
    - energy loss distribution tends towards a Gaussian

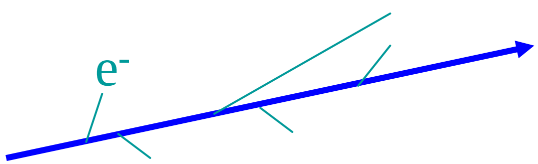

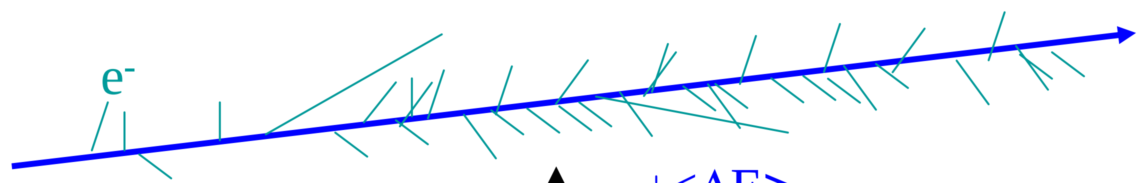

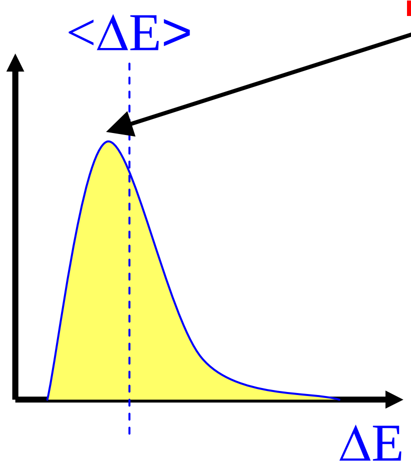

- the most probable loss is often more relevant than the mean energy loss
  - tails are rarer events and often lost in background

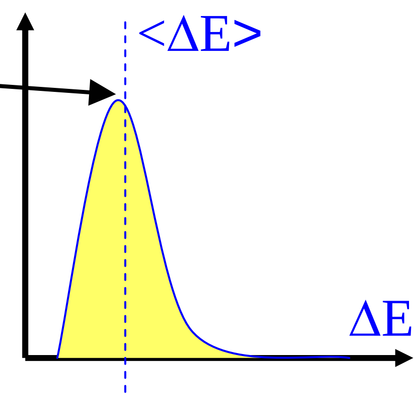

Joram, CERN Summer Student Lectures 2003

Ionization yield

Total ionization

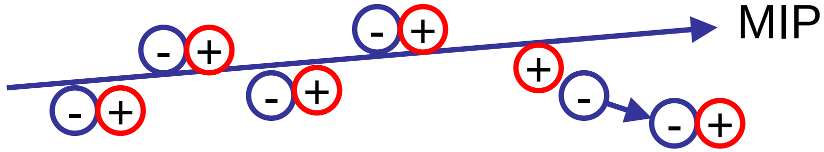

Ar gas: W = 26 eV and
$\Delta E/\Delta x$(MIP) = 2.44 keV/cm
which means n_T = 94 cm^{-1}

- primary ionization electron can have enough kinetic energy to ionize other atoms
- *W*-value: average energy required to form an electron-ion pair

$$n_T = n_p + n_s = \frac{\Delta E}{W} = \text{average total ionization yield}$$

- beware of
  - non-primary electrons leaving the detector
  - W dependence on *E* for slow particles
  - W dependence on contaminants
  - recombination and electron capture

Ionization yield and MIP for gases

Table 4. *Properties of gases at normal conditions: density* ρ, *minimal energy for excitation* E_{ex}, *minimal energy for ionization* E_i, *mean effective ionization potential per atomic electron* $I_0 = I/Z$, *energy loss* W_i *per ion pair produced, minimal energy loss* $(dE/dx)_0$, *total number of ion pairs* n_T *and number of primary ions* n_p *per cm path for minimum ionizing particles* [*SA* 77]

Gas	Z	A	ρ (g/cm³)	E_{ex} (eV)	E_i (eV)	I_0 (eV)	W_i (eV)	$(dE/dx)_0$ (MeV/ g cm⁻²)	$(dE/dx)_0$ (keV/cm)	n_P (cm)⁻¹	n_T (cm)⁻¹
H_2	2	2	8.38×10^{-5}	10.8	15.9	15.4	37	4.03	0.34	5.2	9.2
He	2	4	1.66×10^{-4}	19.8	24.5	24.6	41	1.94	0.32	5.9	7.8
N_2	14	28	1.17×10^{-3}	8.1	16.7	15.5	35	1.68	1.96	(10)	56
O_2	16	32	1.33×10^{-3}	7.9	12.8	12.2	31	1.69	2.26	22	73
Ne	10	20.2	8.39×10^{-4}	16.6	21.5	21.6	36	1.68	1.41	12	39
Ar	18	39.9	1.66×10^{-3}	11.6	15.7	15.8	26	1.47	2.44	29.4	94
Kr	36	83.8	3.49×10^{-3}	10.0	13.9	14.0	24	1.32	4.60	(22)	192
Xe	54	131.3	5.49×10^{-3}	8.4	12.1	12.1	22	1.23	6.76	44	307
CO_2	22	44	1.86×10^{-3}	5.2	13.7	13.7	33	1.62	3.01	(34)	91
CH_4	10	16	6.70×10^{-4}		15.2	13.1	28	2.21	1.48	16	53
C_4H_{10}	34	58	2.42×10^{-3}		10.6	10.8	23	1.86	4.50	(46)	195

Kleinknecht

Ionization fluctuations

Fano factor

- naively expect $\sigma^2(n_T) = n_T$ (Poisson)
- But for a given energy deposition, n_T is limited by energy conservation, so the fluctuations are in fact smaller

Table 1.3. *Fano factors for typical detector materials [54]*

source	energy	absorber	F
X-rays	5.9 keV	Ar + 10 % CH_4	0.21
"	2.6 keV	"	0.31
α	5.03 MeV	"	0.18
α	5.68 MeV	Ar + 0.8 % CH_4	0.19
p	1 . . . 4.5 MeV	Si	0.16

Grupen

$$\sigma^2(n_T) = F n_T$$

Ionization chambers

Parallel electrodes

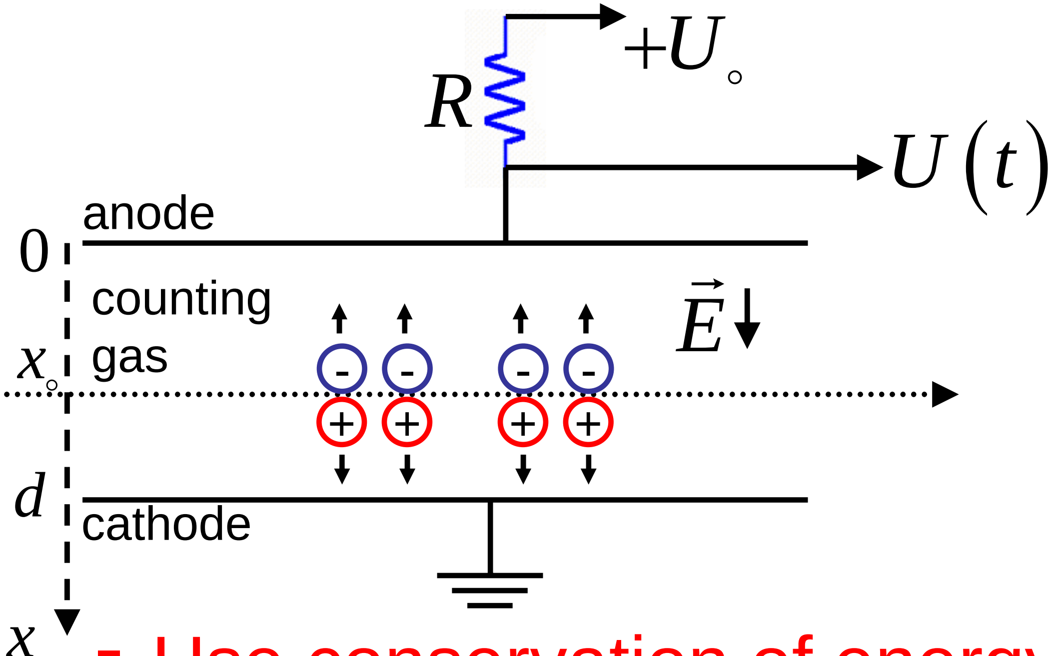

$$\left|\vec{E}\right| = \frac{U(t)}{d} \qquad C = \frac{\varepsilon A}{d}$$

$$\int_0^{t_d^-} v^- dt = x_\circ$$

$$\int_0^{t_d^+} v^+ dt = d - x_\circ$$

$$v^+ < v^-$$

drift velocities depend on the electric field

- Use conservation of energy in C

$\frac{1}{2} C U_\circ^2 = \frac{1}{2} C U^2(t) +$ work done by $\vec{E}$ on drifting charges

obtain $$-\frac{dU(t)}{dt} = \frac{Ne}{Cd}\left[v^- + v^+\right]$$

holds for $v = v\left(\left|\vec{E}\right|(t)\right)$

Ionization chambers

Signal

$$\Delta U(t) = U(t) - U_\circ = \Delta U^-(t) + \Delta U^+(t)$$

$$-\Delta U(t_d^+) \equiv -\Delta U = \frac{Ne}{Cd}\left[x_\circ - (d - x_\circ)\right] = \frac{Ne}{C}$$

$$\Delta Q = -Ne = C\Delta U$$

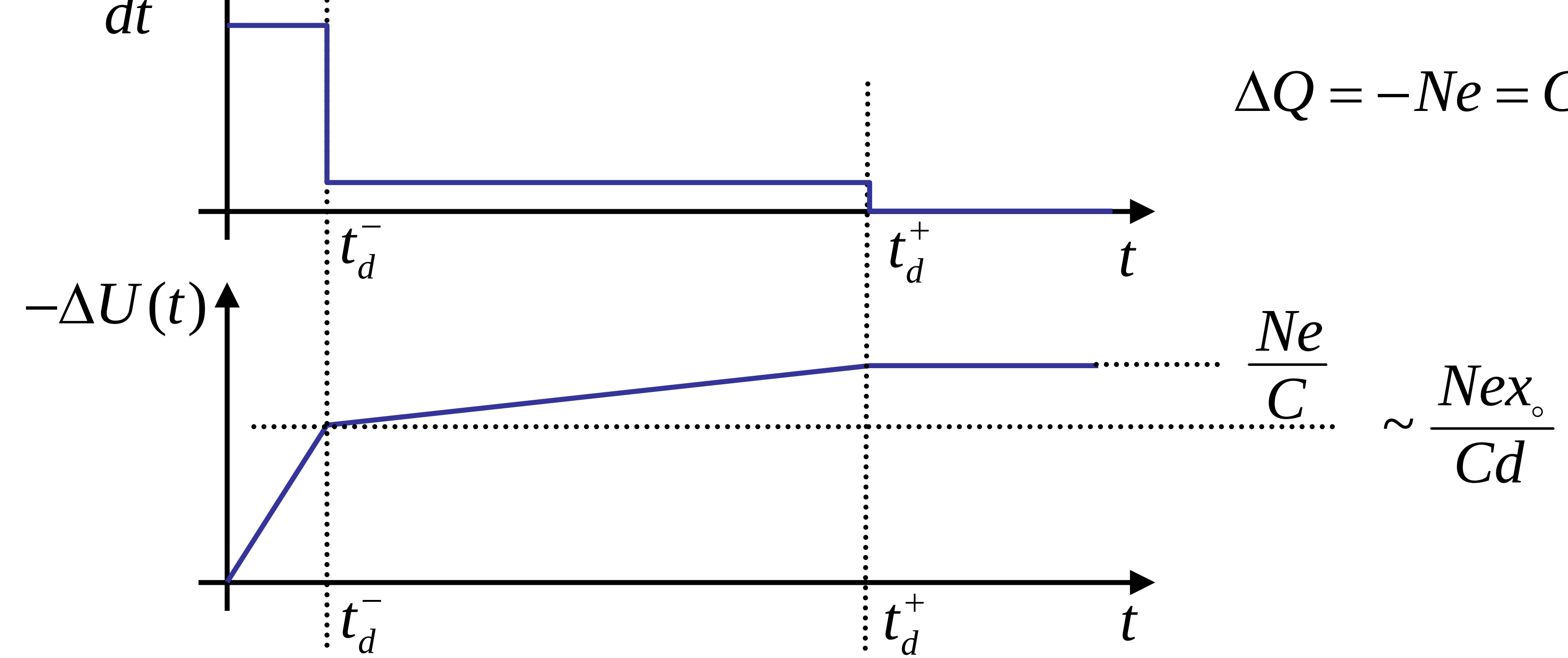

$$\frac{\Delta U^+}{\Delta U^-} = \frac{d - x_\circ}{x_\circ}$$

If $x_\circ = \frac{1}{2}d$ then $\frac{\Delta U^+}{\Delta U^-} = 1$

Ionization chambers

Frisch grid

- problem: in practice one does not want to wait so long to have a signal independent of x_o
  - solve this problem by mounting a grid between anode and cathode, at some intermediate potential

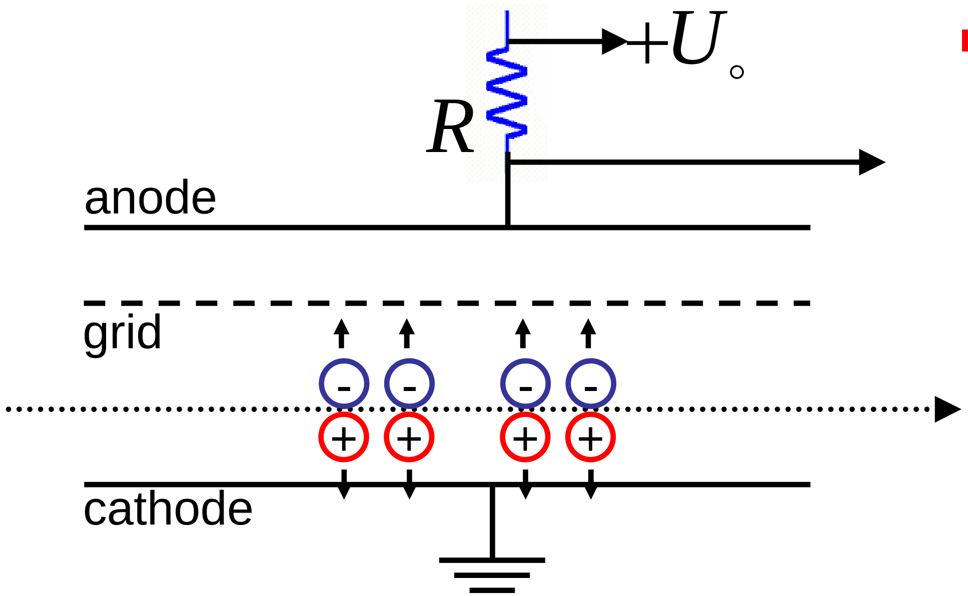

- How does this solve the problem?

Ionization chambers

Bias resistor

- results valid for *RC* >> drift times
- for finite *R*, need to consider the recharging of *C*

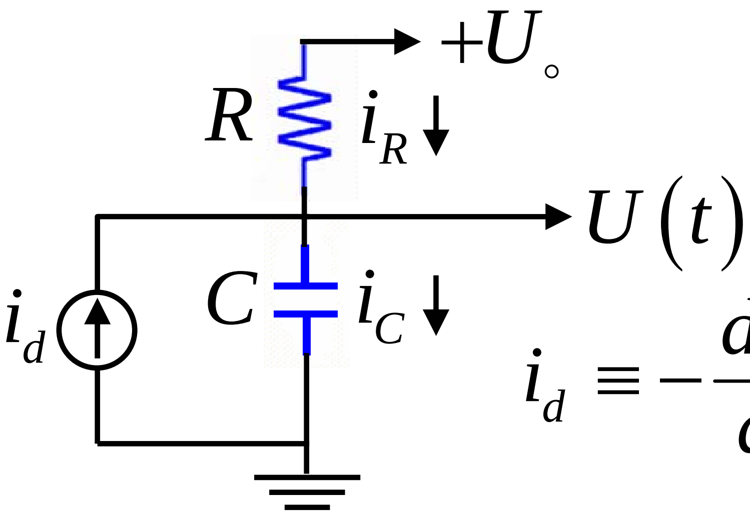

$$i_R = i_C + i_d$$

$$i_d \equiv -\frac{dQ}{dt}\bigg|_{\text{due to drift}} = -C\frac{dU}{dt} = \frac{Ne}{d}\left[v^- + v^+\right]$$

If $RC \gg t_d^-$ but $RC < t_d^+$ on obtains

$$-\Delta U\left(t_d^+\right) = \frac{Ne}{Cd}x_\circ + \frac{Ne}{d}v^+ R\left[1 - \exp\left(-\frac{t_d^+}{RC}\right)\right]$$

Ionization chambers

Cylindrical electrodes

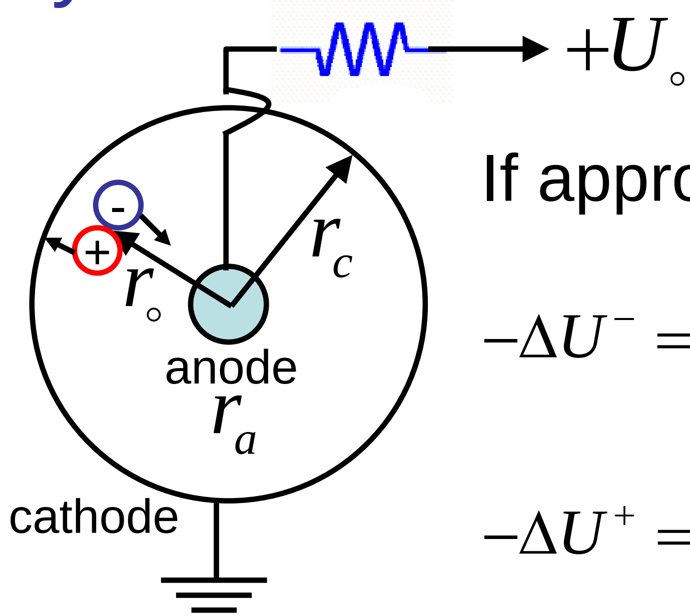

$$\left|\vec{E}(r)\right| = \frac{U}{r\ln\frac{r_c}{r_a}} \propto \frac{1}{r}$$

If approximation $v^{\pm} \propto \left|\vec{E}\right|$ then

$$-\Delta U^- = \frac{Ne}{C}\frac{(\ln r_\circ - \ln r_a)}{(\ln r_c - \ln r_a)}$$

$$-\Delta U^+ = \frac{Ne}{C}\frac{(\ln r_c - \ln r_\circ)}{(\ln r_c - \ln r_a)}$$

$$\Delta U = \Delta U^- + \Delta U^+ = -\frac{Ne}{C}$$

$$\Delta Q = -Ne = C\Delta U$$

$$\frac{\Delta U^+}{\Delta U^-} = \frac{\ln r_c - \ln r_\circ}{\ln r_\circ - \ln r_a}$$

If $r_\circ = \frac{2}{3} r_c$ and $r_a \ll r_c$ then $\frac{\Delta U^+}{\Delta U^-} = \frac{\ln\frac{3}{2}}{\ln\frac{2r_c}{3r_a}} < 1$

for $r_c = 1$ cm and $r_a = 30$ µm then $\frac{\Delta U^+}{\Delta U^-} = 0.075$

- in general electrons contribute more to the signal
- discharging *C*: pocket dosimeter

Silicon detectors

- Solid state ionization detector
  - traversing charged particle creates e^--hole pairs
    - also photo-e^- caused by a photon
  - low *dE/dx* required to produce pairs
    - Si: 3.6 eV   Ge: 2.9 eV
    - gases: 20 eV to 40 eV
    - scintillators: 400 eV to 1000 eV for light $\rightarrow$ 1 photo-e^-
  - electric field across the junction causes e^--hole to drift apart, producing a detectable current

Silicon detectors

The p-n junction

A. Peisert, Instrumentation In High Energy Physics, World Scientific

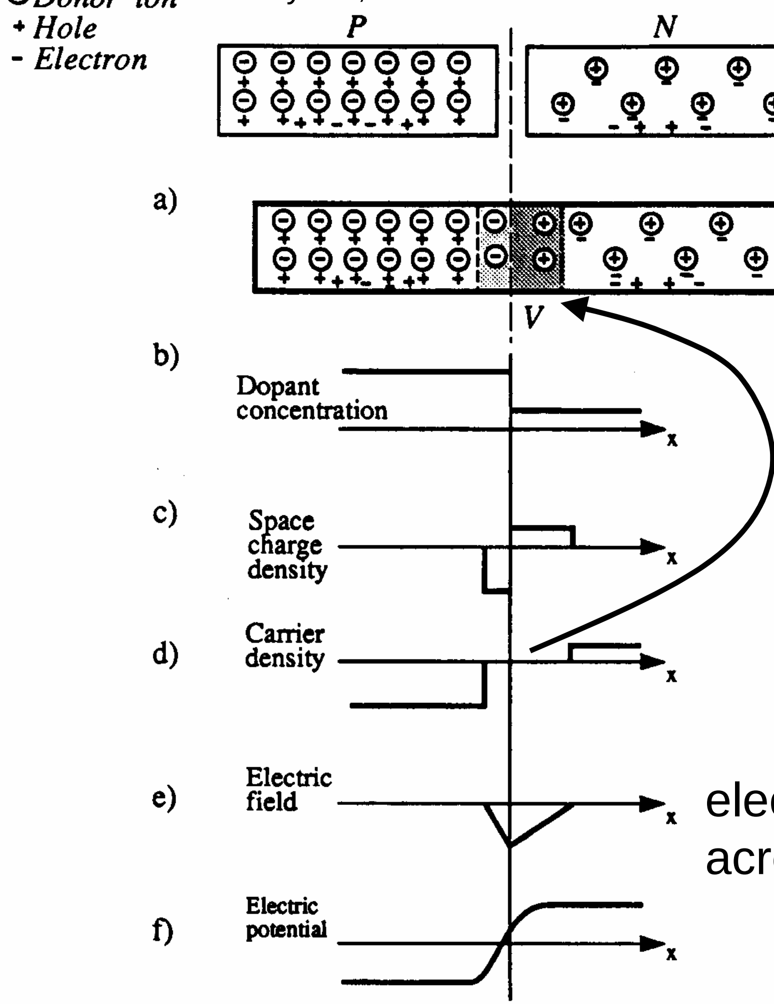

p: doped with electron-acceptor ions
n: doped with electron-donor ions

diffusion of e^- into the p zone
diffusion of holes into the n zone

depleted zone

electric field across junction

Applying a reverse bias voltage further depletes the junction, and provides an electric field sufficiently large to allow signal collection before the e^--ion pairs recombine

Silicon detectors

- Silicon microstrip (A. Peisert, Instrumentation In High Energy Physics, World Scientific)
  - spatial information by segmenting the p layer
  - technology extensively used in trackers
    - First hadron collider use in UA2
  - pixel segmentation for fine 2D readout
  - ATLAS and CMS use Si microstrips and pixels

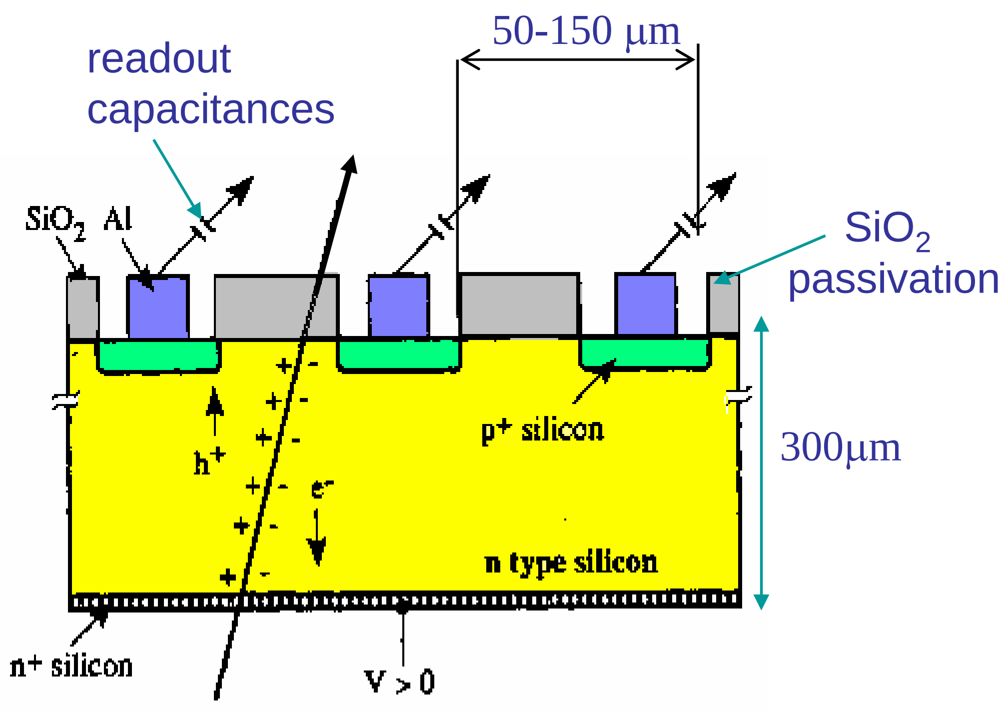

Proportional counters

Gas amplification

- ionization chambers yield small signals
  - MIP in 1cm thick Ar gas detector: about 100 e-ion pairs
  - compare with typical amplifier noise of 1000 e^- (ENC)
- strong electric field close to anode

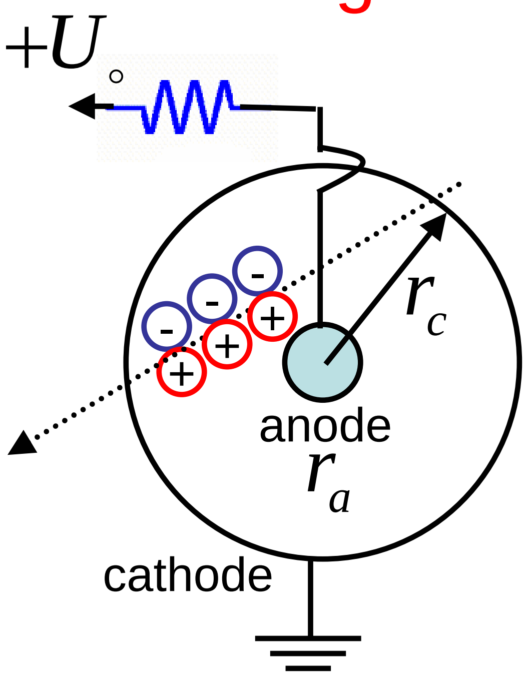

- electrons can gain enough kinetic energy (between collisions, while drifting) to further ionize the gas
- exponential increase of the number of e-ions pairs

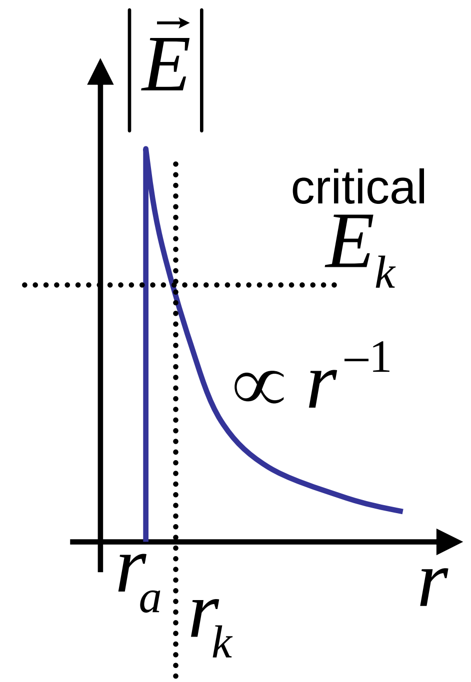

Proportional counters

1st Townsend coefficient α

$$\alpha = \sigma_{\text{ion}} \frac{N_A}{V_{\text{mol}}} = \lambda^{-1}$$

mean free path λ

$$V_{\text{mol}} = 22.4 \text{ liter/mol}$$

$$dn(r) = \alpha(r)\, n(r)\, dr$$

$$\Rightarrow \quad n = n_\circ \exp\left(\int_{r_a}^{r_k} \alpha(r)\, dr\right)$$

- it holds that

$$\Delta U = -\frac{e}{C} n_\circ A$$ proportional to n_o

$$A = \frac{n}{n_\circ}$$ gain

$$A = \exp\left(\int_{r_a}^{r_k} \alpha(r)\, dr\right) \simeq k \exp\left(\frac{U_\circ}{U_{\text{ref}}}\right)$$

Kleinknecht

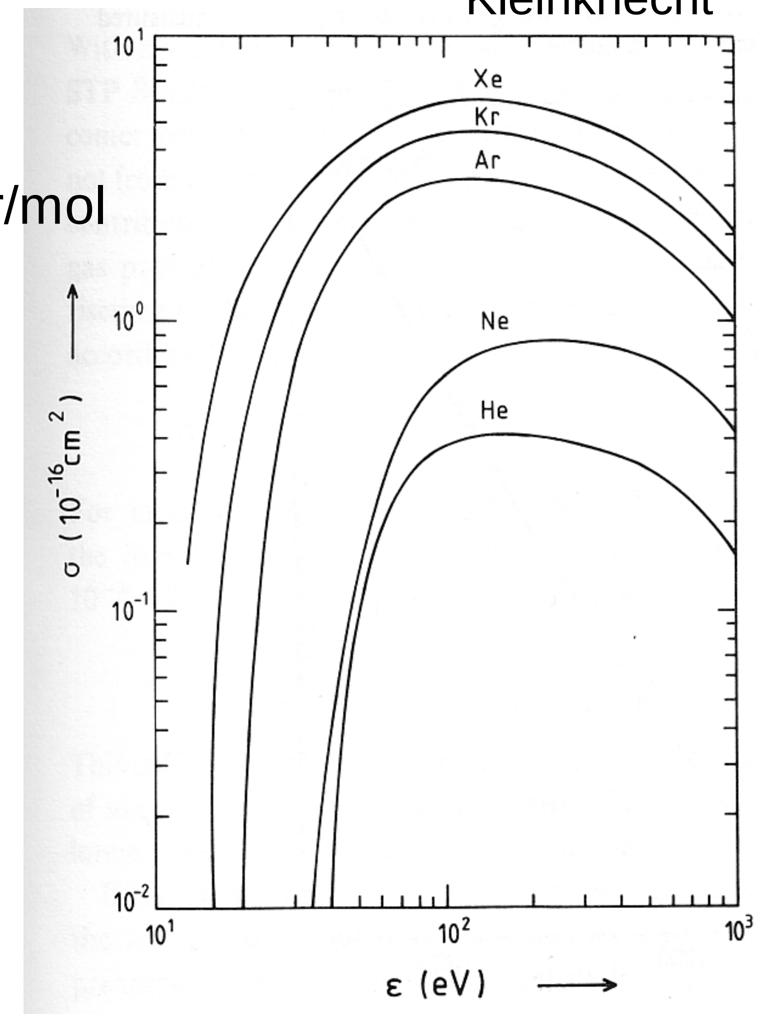

Proportional counters

- 2^{nd} Townsend coefficient γ
  - electrons in the avalanche can excite atoms, which then emit photons
  - these photons can produce further electrons through the photoelectric effect

$$A_\gamma = \frac{n}{n_\circ} = \frac{A}{1-\gamma A}$$

gain including the effect of photons

    - quenching gas (organic molecule with large photo-absorbtion σ) can absorb most photons and keep the avalanche localized
  - for $\gamma A \to 1$, the signal amplitude is ind of n_o: end of proportional regime

Proportional counters

Signal formation

- saturation effects eventually terminates the avalanche

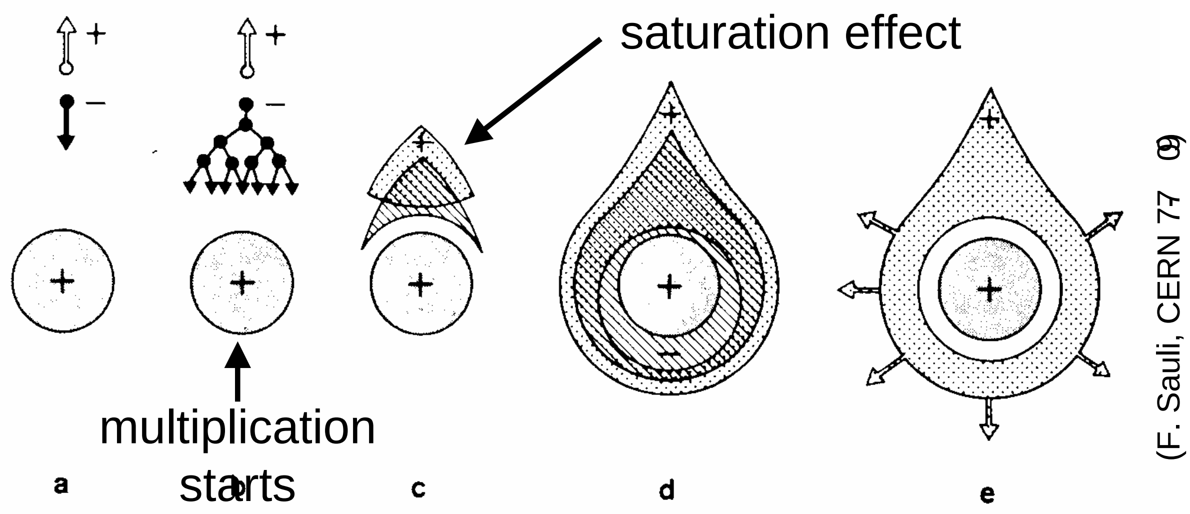

- typical values

$$r_c = 1\ \text{cm},\quad r_a = 30\ \mu\text{m},\quad r_k = 50\ \mu\text{m} \quad\Rightarrow\quad \frac{\Delta U^+}{\Delta U^-} = \frac{\ln r_c - \ln r_k}{\ln r_k - \ln r_a} = 10.4$$

- electrons collected by the wire in a few ns
- the ions contribute to most of the signal, but their contribution comes much later
- needs signal differentiation to limit dead time

Proportional counters

Signal shape

- current source $I(t) = Q\frac{d}{dt}F(t)$
- voltage source $U(t) = \frac{Q}{C}F(t)$

Q: positive charge in the avalanche

$$F(t) = \frac{\ln\left(1+\frac{t}{t_\circ}\right)}{\ln\left(1+\frac{t_{max}}{t_\circ}\right)}$$

$t_\circ$: a few ns

t_{max}: a few μs, the time it takes ions to reach the cathodes

Straw tubes

- Cylindrical proportional chamber of small (less than 1cm) diameter are perfect straw-detector units: used in ATLAS Transition radiation Tracker

Cylindrical gas detectors

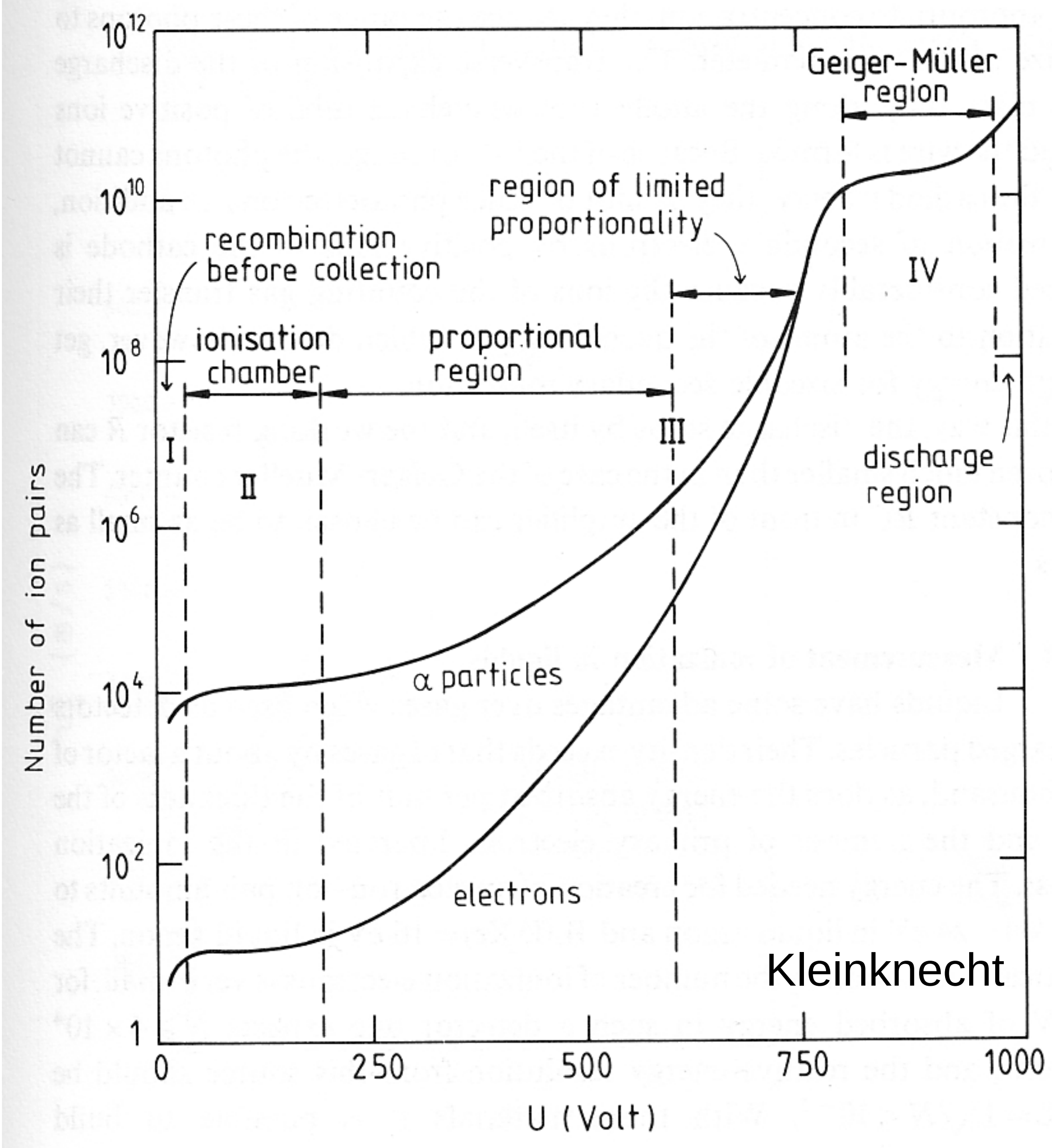

Multi wire proportional chambers

- Charpak et al. 1968. (Nobel prize 1992)
  - before MWPC, tracking used optical means
  - breakthrough: each wire in a MWPC acts as an independent proportional counter
    - negative pulse on wire 1 caused by capacitive coupling with negative pulse on parallel neighbour wire 2 is compensated by the positive signal induce on wire 1 by the positive ions moving away from 2 towards 1
    - electrons produced in the avalanche are collected by the wires in a few ns
    - ions drift away from the wires and generate a signal which can be amplified

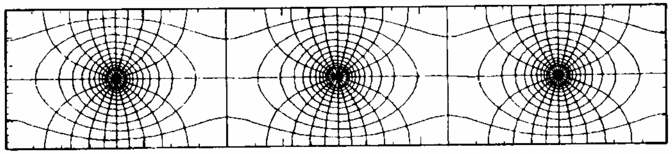

field lines and equipotentials around anode wires

Multi wire proportional chambers

- Typical parameters
  - with digital readout: $\sigma_x = \frac{d}{\sqrt{12}}$

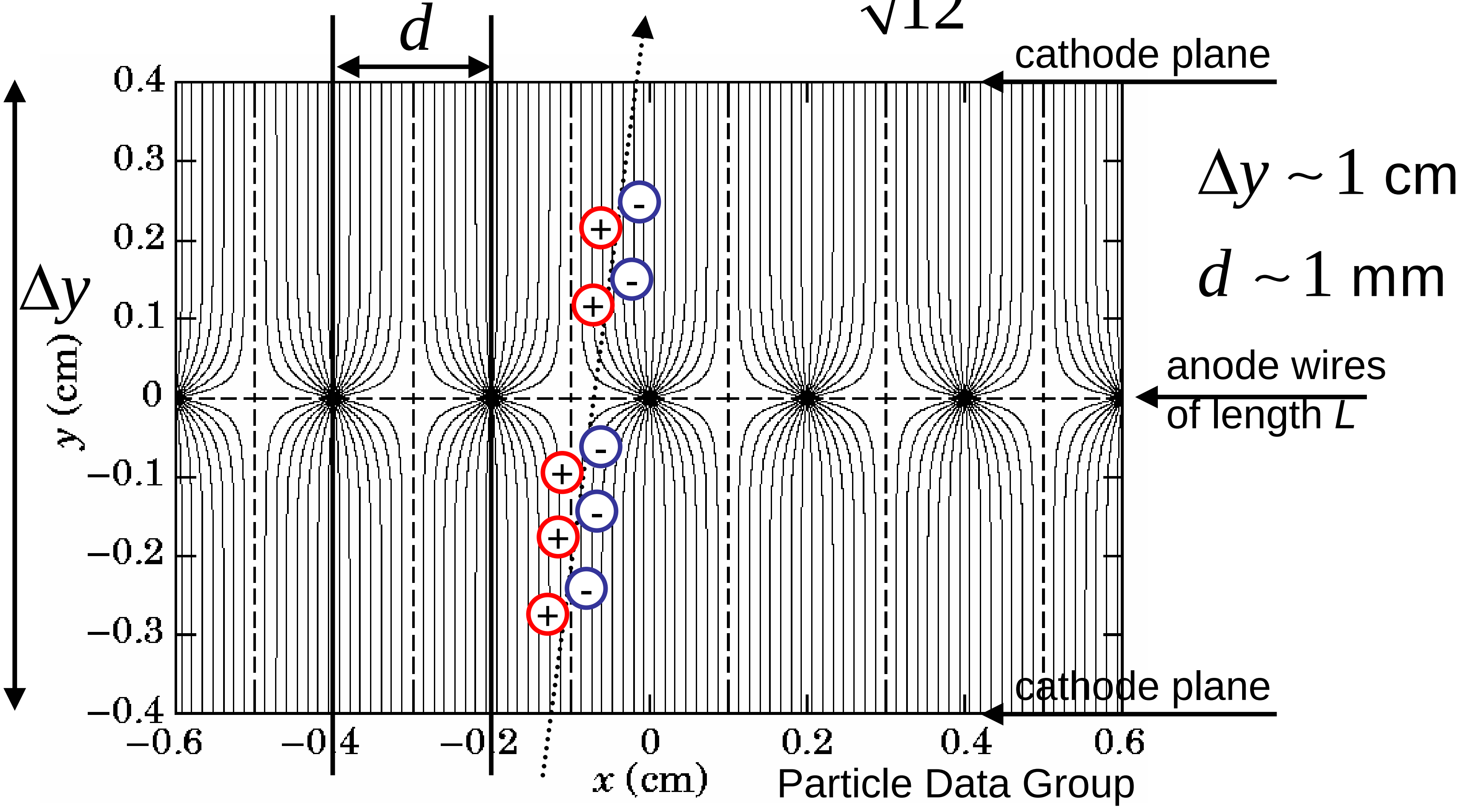

Multi wire proportional chambers

- Fundamental limitation
  - electrostatic force between wires is balance by the mechanical tension *T;* mechanical stability requires $T \geq T_o \propto U_o^2$; wires have elastic limit!
- Secondary coordinate
  - Crossed wire planes
    - ghost hits; restricted to low multiplicities
  - Charge division (at end of wires)
    - resistive wires (carbon, 2kΩ/m); $\sigma(y/L) < 0.4\%$
  - Timing difference (of signal at end of wires)
    - $\sigma(\Delta t) = 0.1$ ns provides $\sigma(y) \approx 4$ cm (OPAL)
  - Segmented cathode planes

Derivatives of proportional chambers

Thin gap chamber (TGC)

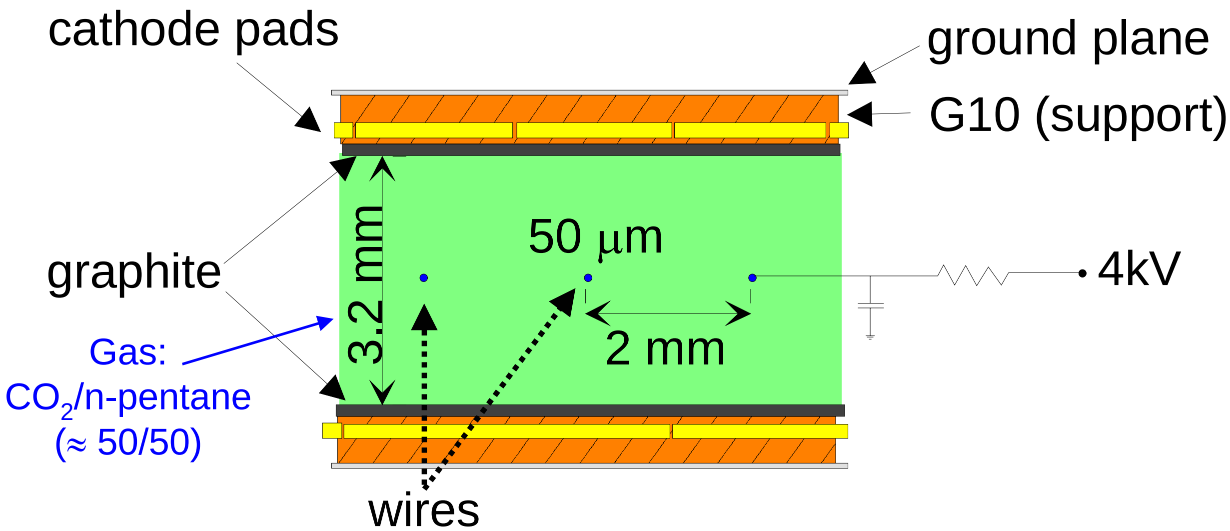

- Operation in saturated mode. Resistivity of graphite layer limits the signal amplitude
- fast (2 ns risetime), large signal, robust
- ATLAS muon endcap trigger Y.Arai et al. NIM A 367 (1995) 398

Derivatives of proportional chambers

- Resistive plate chamber (RPC)
  - No wires!

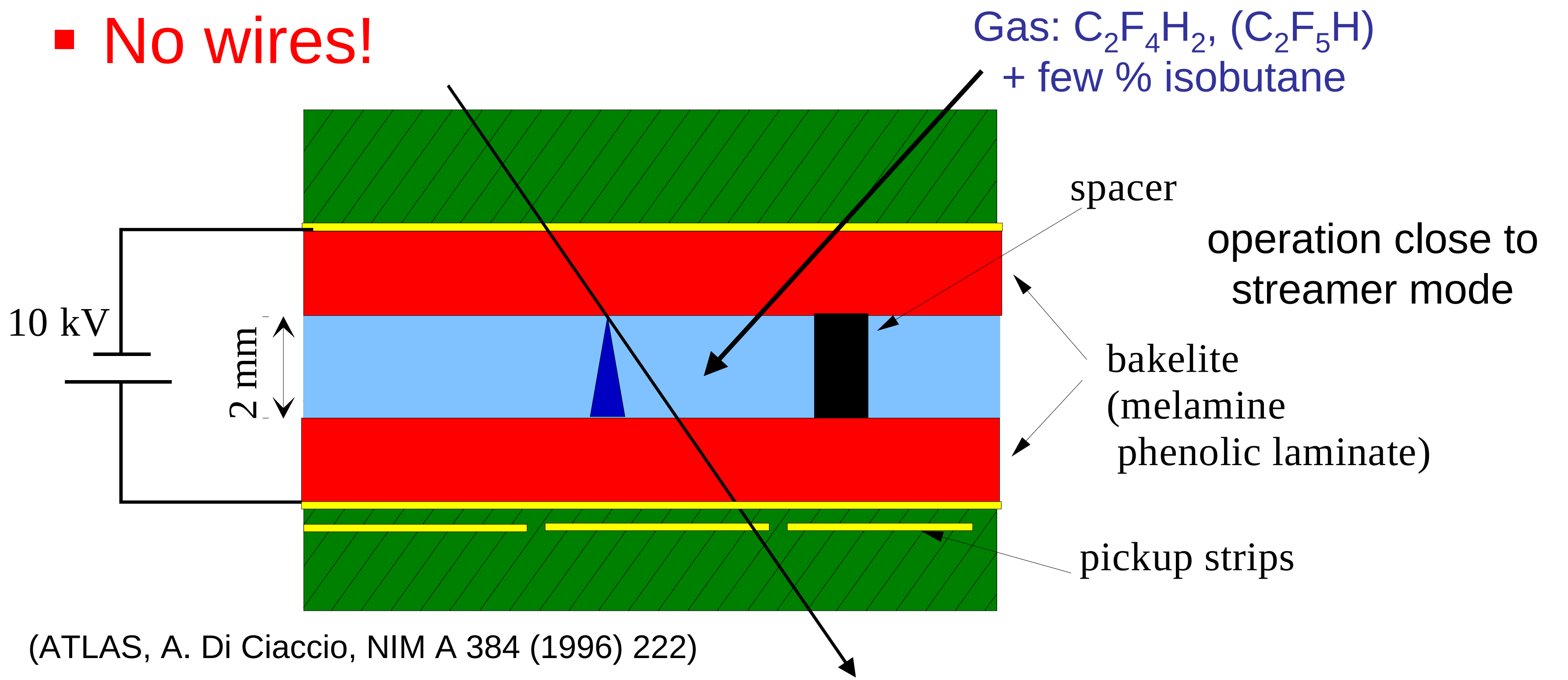

(ATLAS, A. Di Ciaccio, NIM A 384 (1996) 222)

  - Small time dispersion, under 2 ns, and high rate capability, up to 1 kHz/cm^2
  - ATLAS barrel muon system

Drift chambers

Concept

- Proportional chamber with measurement of drift time added (First studies: T. Bressani, G. Charpak, D. Rahm, C. Zupancic, 1969 First operation drift chamber: A.H. Walenta, J. Heintze, B. Schürlein, NIM 92 (1971) 373)

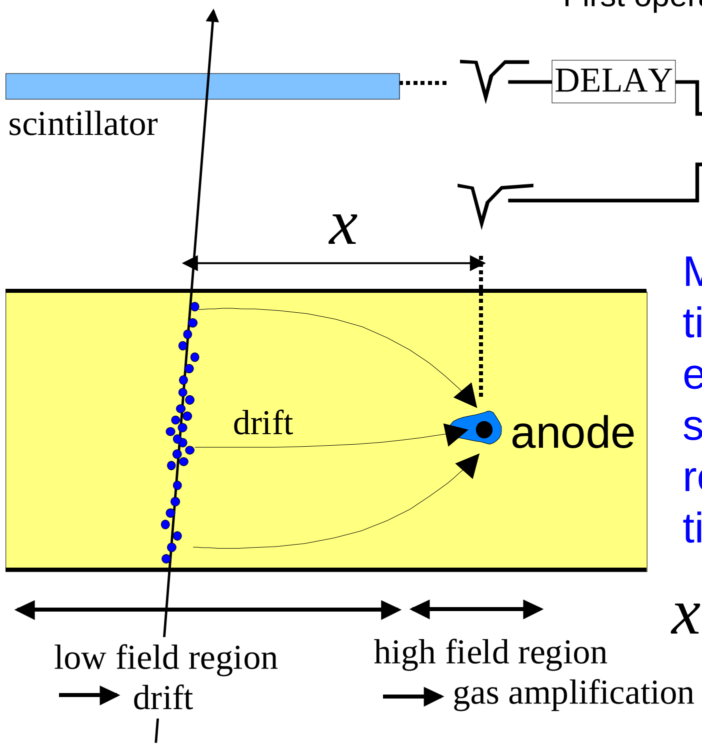

Measure arrival time of electrons at sense wire relative to a time t_0.

$$x = \int v^{-}(t)dt$$

- space resolution not limited to cell size
- Anodes typically 5 to 10 cm apart, corresponding to 1 to 2 ms drift time, yielding $\sigma_x \approx 50$ to 100 μm
- Resolution limited by
  - field uniformity
  - diffusion

- ATLAS muon system precision tracking is done with Monitored Drift Tubes (MDT)

Drift and diffusion in gases

- No external fields
  - Electrons and ions lose their energy due to collisions with the gas atoms

$$\varepsilon = \tfrac{3}{2}kT \approx 40\ \text{meV}$$

thermalization and Maxwell-Boltzmann energy distribution

$$\frac{dN}{Ndx} = \frac{1}{\sqrt{4\pi Dt}} \exp\left\{-\frac{x^2}{4Dt}\right\}$$

spreading of localization

D: diffusion coefficient

$$\sigma_x(t) = \sqrt{2Dt} \qquad \sigma_{3D}(t) = \sqrt{6Dt}$$

Drift and diffusion in gases

External electric field

$$\vec{v} = \mu \vec{E}$$

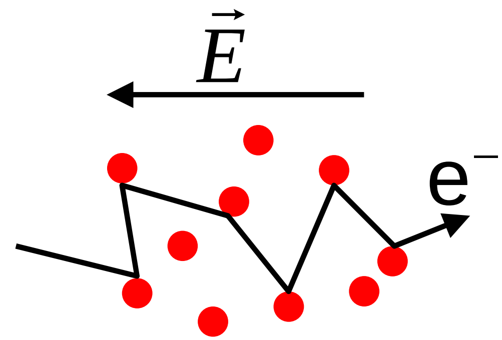

- "stop and go" traffic in gas atoms

$$v^2 = \frac{e\left|\vec{E}\right|}{m N_g \sigma_{col}(\varepsilon)} \sqrt{\tfrac{1}{2}\Delta(\varepsilon)}$$

N_g is the number of gas molecules per unit volume

fractional e energy loss per collision

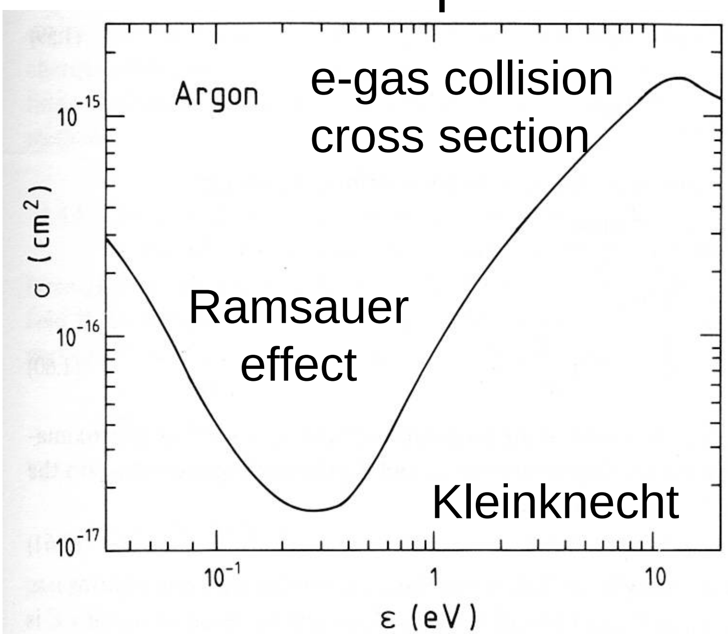

ion drift velocities about 1000 lower

$$D_T^E = D$$

$$D_L^E \approx D$$

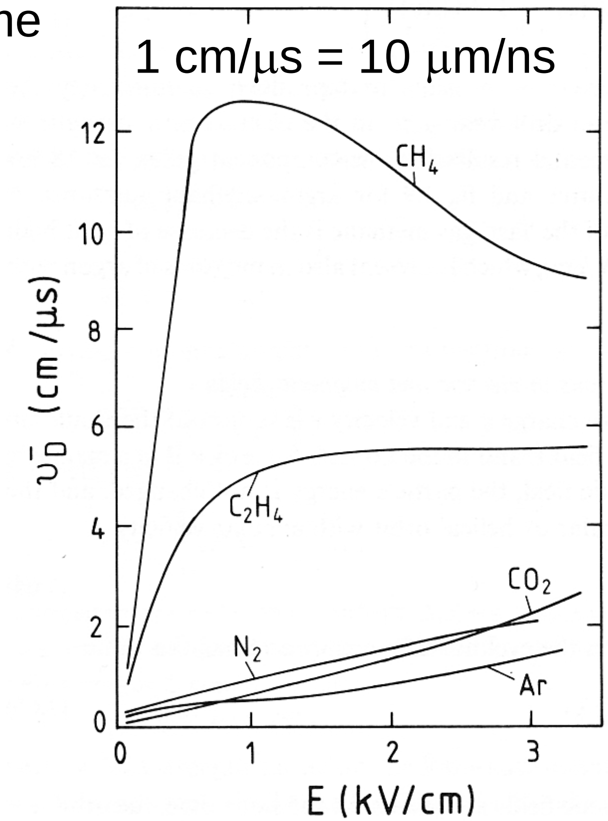

Drift and diffusion in gases

External electric and magnetic fields

- drift and diffusion driven by $\vec{E} \times \vec{B}$ effects
- case $\vec{E} \perp \vec{B}$

time between two collisions → $\tau = \left\langle \frac{1}{N_g \sigma_{col}(\varepsilon) u} \right\rangle$ ← instantaneous velocity

$$\omega = \frac{e|\vec{B}|}{m}$$ cyclotron frequency

$$\tan \alpha_L = \omega\tau$$

Lorentz angle

$$v = \frac{\mu|\vec{E}|}{\sqrt{1+\omega^2\tau^2}}$$

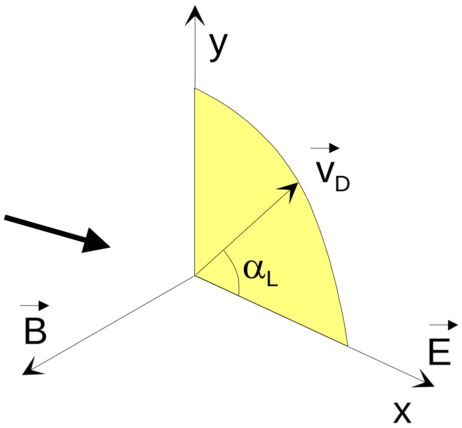

drift at an angle with respect to the electric field

Drift and diffusion in gases

External electric and magnetic fields

- diffusion transverse to magnetic field is reduced
  - electrons are forced on circle segments with $r = u_T/\omega$
  - the diffusion coefficient transverse to the magnetic field appears reduced

$$D_T^B = \frac{D}{1+\omega^2\tau^2}$$

- case $\vec{E} \parallel \vec{B}$
  - the drift is as for the electric case
  - the diffusion transverse to the drift is reduced!

Drift chambers

Planar drift chamber designs

Optimize the geometry for constant electric field

Choose drift gases with small E field dependence

Aim at a linear relation between space and time for drifting electrons

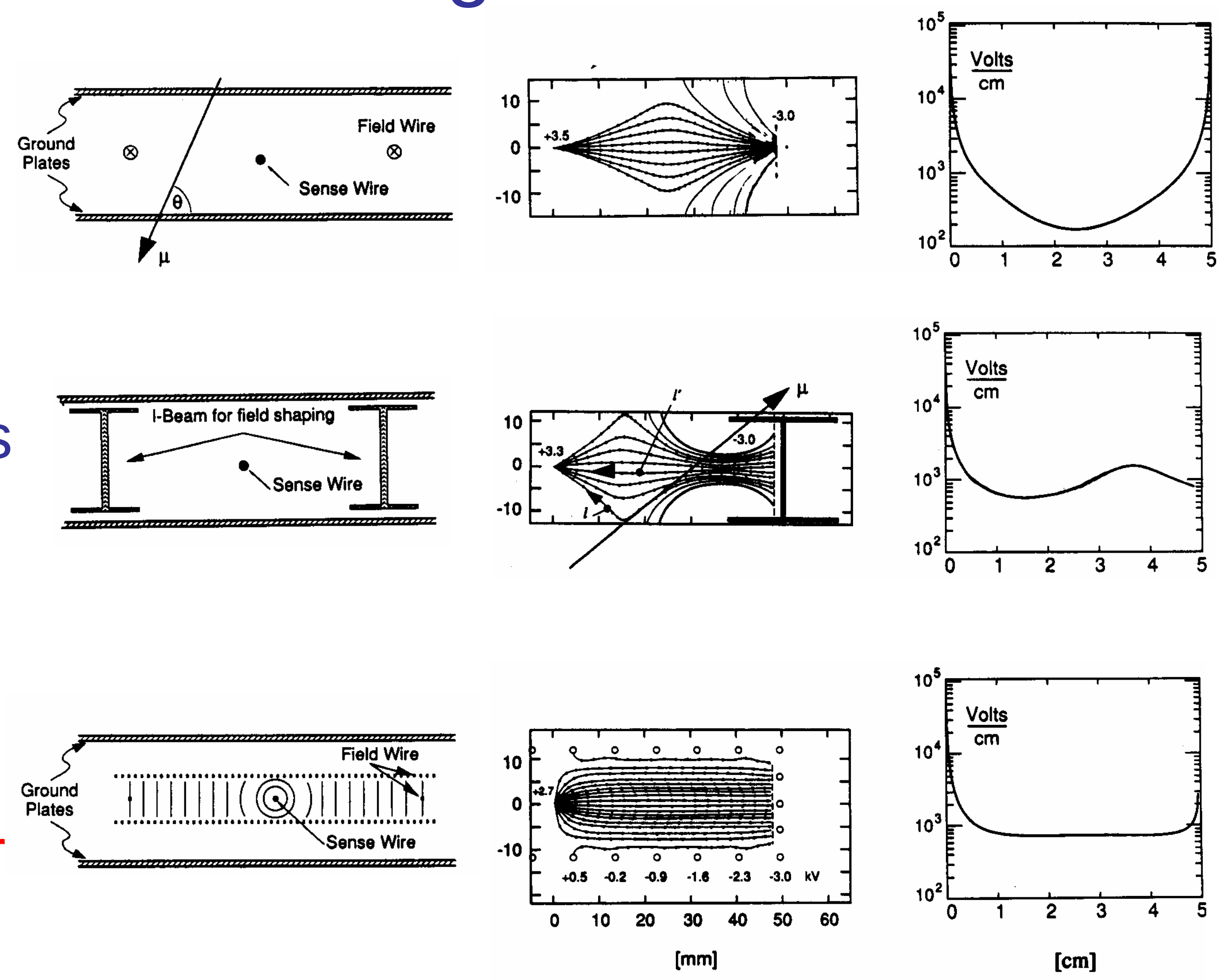

(U. Becker, in: Instrumentation in High Energy Physics, World Scientific)

Drift chambers

Cylindrical drift chambers

- Position resolution determined by
  - diffusion, path fluctuations
  - electronics
  - primary ionization statistics

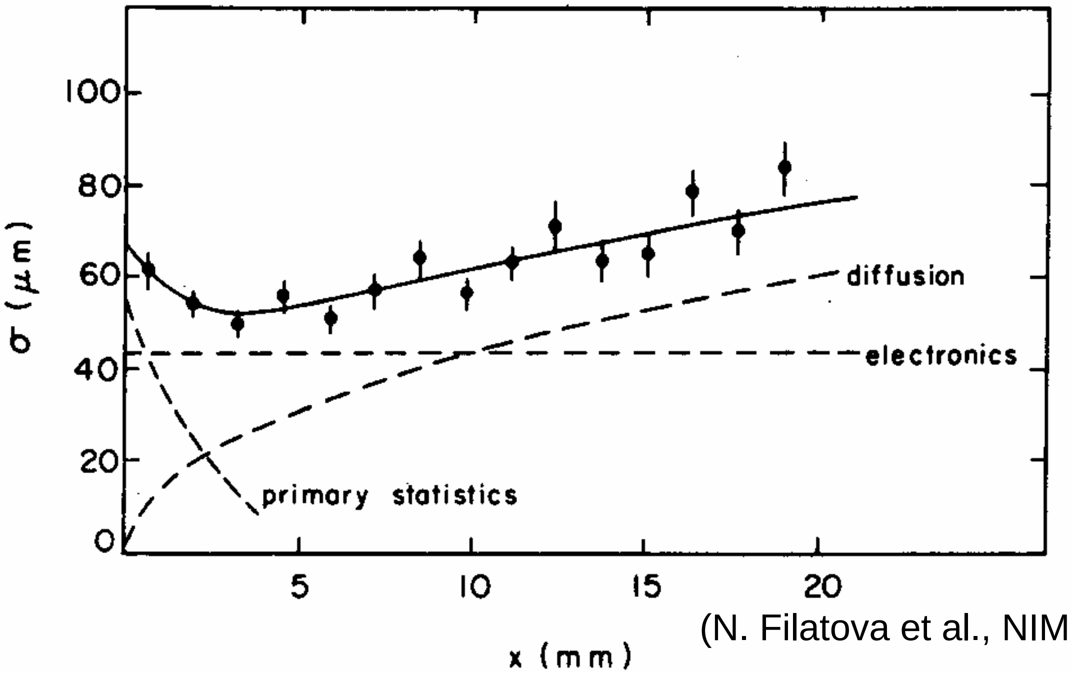

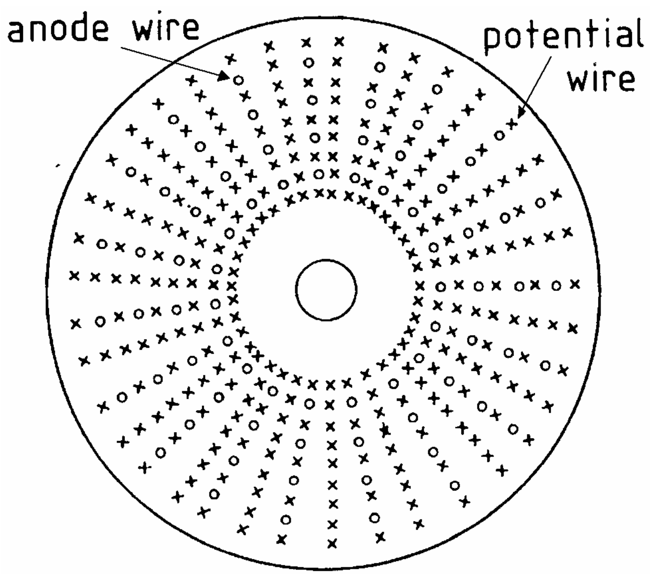

(N. Filatova et al., NIM 143 (1977) 17)

Drift chambers

Geometries of cylindrical drift chambers

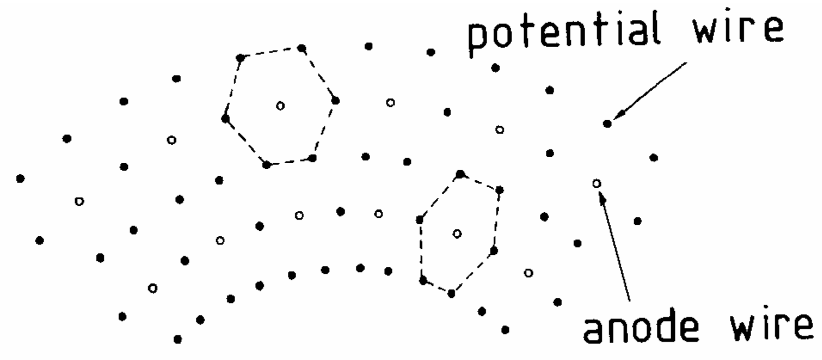

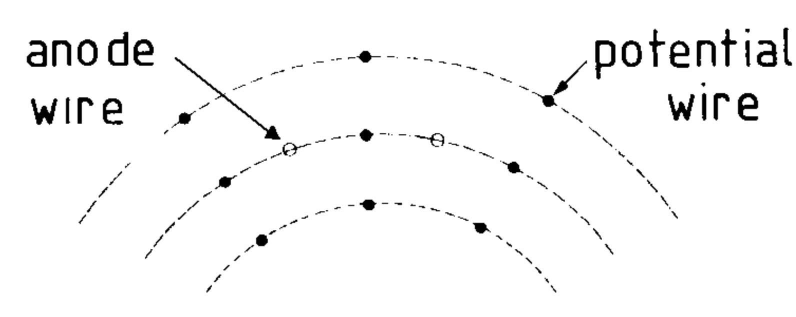

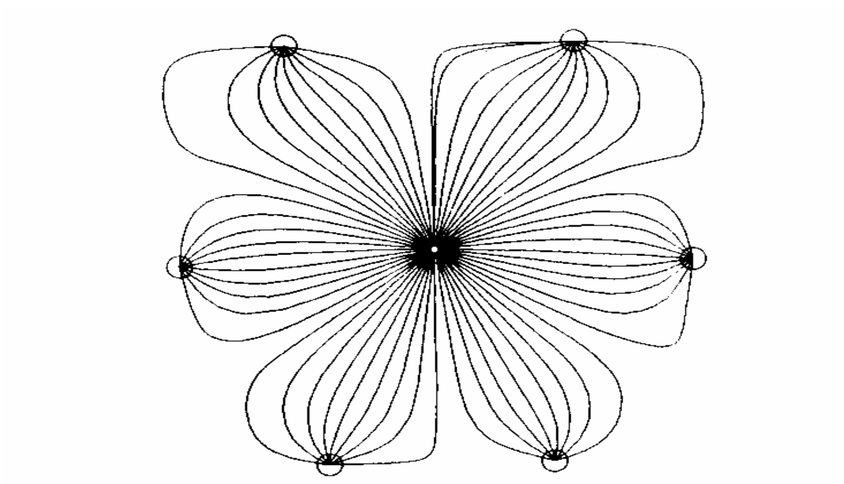

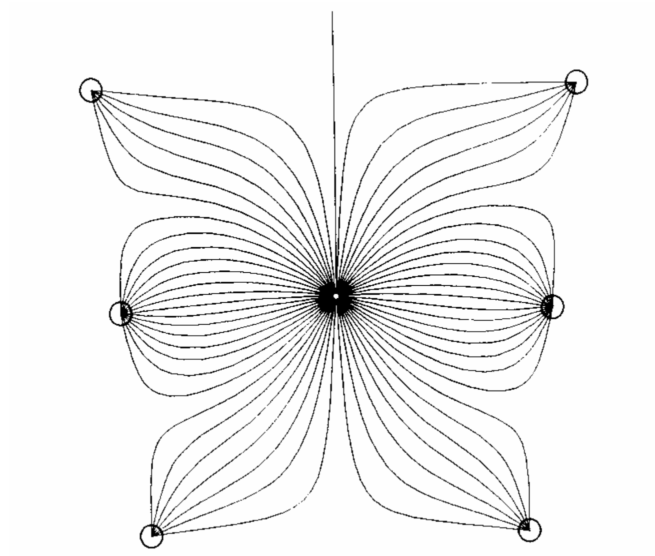

Drift chambers

Time projection chamber

- Optimal chamber including all features

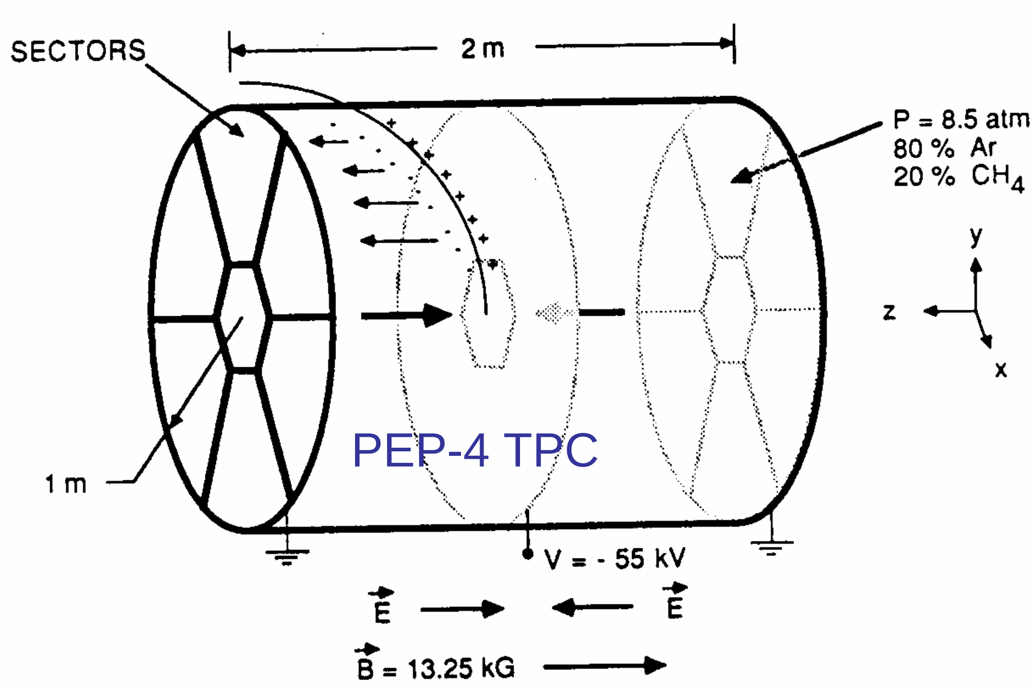

- x-y from signal readout at the end plates
- z from drift time
- analog readout provides *dE/dx* information
- magnetic field provides momentum and reduce transverse diffusion

- drift over long distances requires good gas quality, precise knowledge of the drift velocity, careful tuning of drift field
- control space charge problems with ion stopping grids (gates)

Micro gaseous detectors

Microstrip gas chambers (MSGC)

(A. Oed, NIM A 263 (1988) 352)

- Improve speed and resolution with smaller device
  - reproduce the field structure of MWPC with a significant scale reduction
  - metallic anode and cathode strips typically 100 to 200 μm apart on an insulating support
  - fast ion evacuation: high rate capability up to 10^6 mm^{-2}s^{-1}
  - resolution 30 - 40 μm

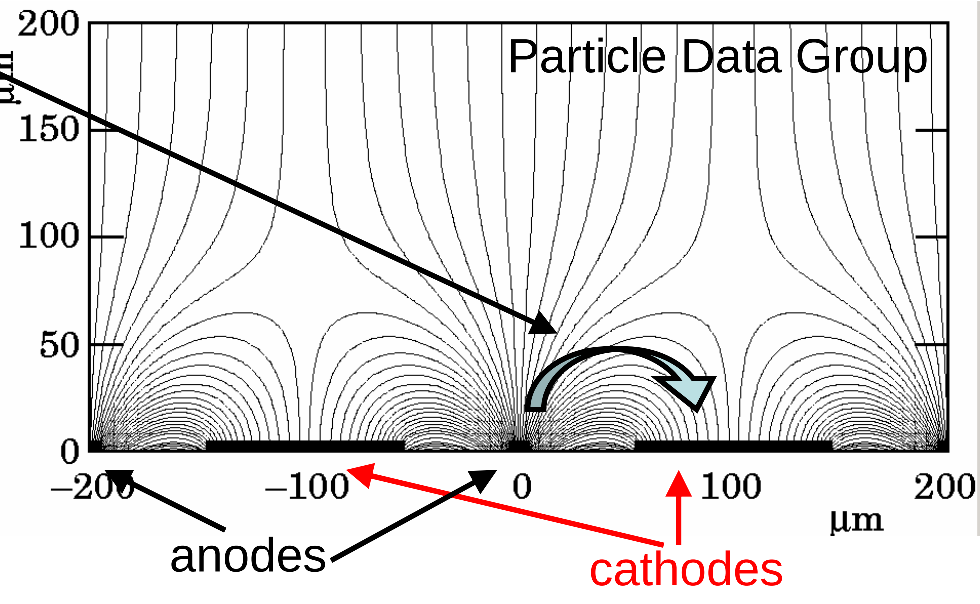

Micro gaseous detectors

- Gas electron multiplier (GEM) (R. Bouclier et al., NIM A 396 (1997) 50)
  - thin metal-clad polymer foil, chemically pierced by a high density of holes
  - electrons drift into holes, multiply, and get out

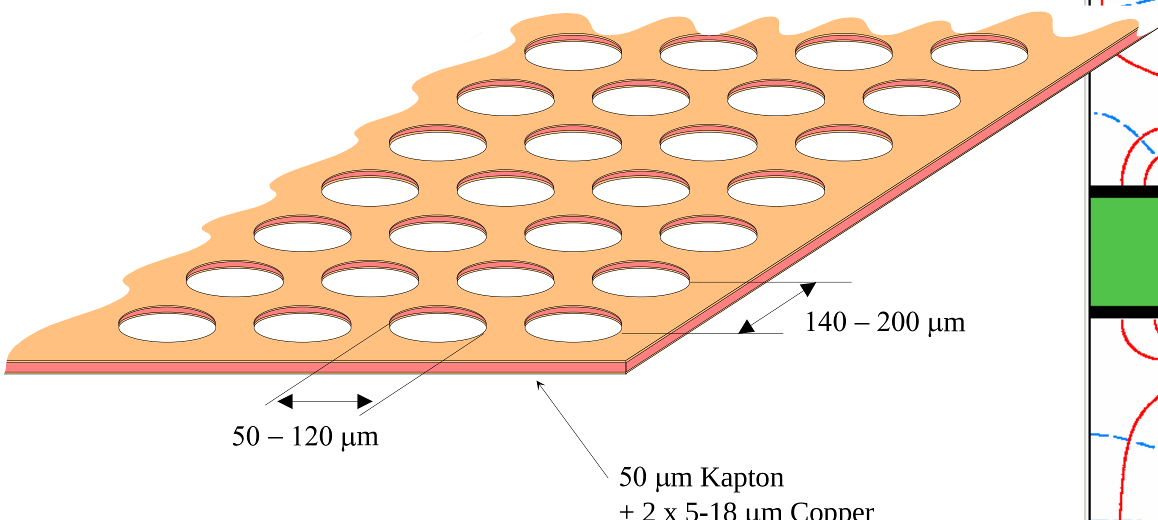

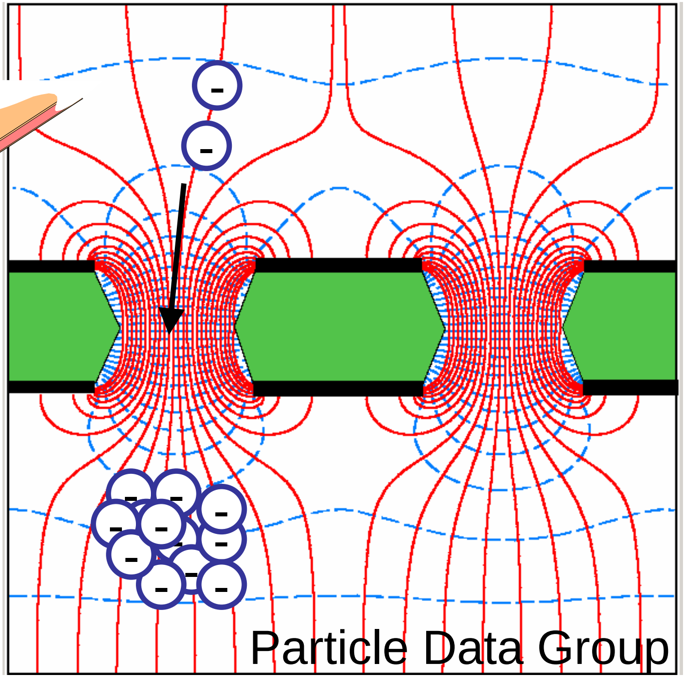

Micro gaseous detectors

- TPC with GEM and pad readout (D. Karlen et al., NIM A 555 (2005) 80-92)
  - electrons first drift in large drift volume
  - electron multiplication in multiple stage GEM
  - induced signal read out on PCB pads

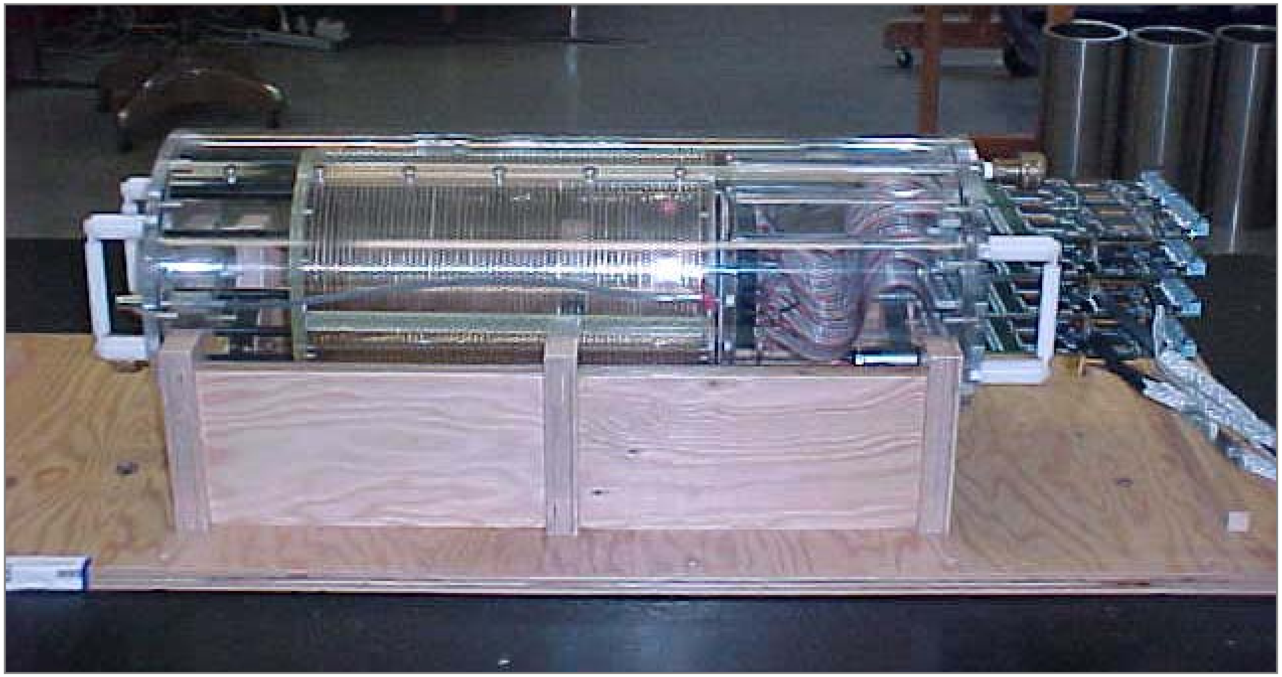

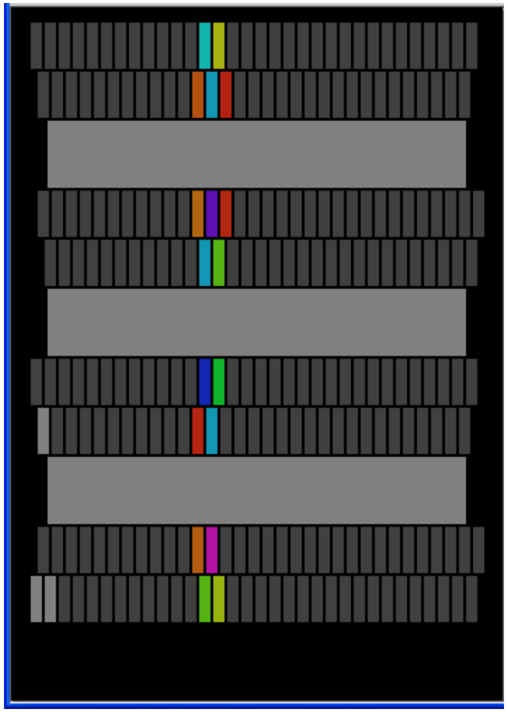

Lecture I: Questions

- Question I.1
  - Consider the parallel electrode ionization chamber with a Frish grid. Explain how a Frisch grid solves the problem mentioned on slide I/15.
- Question I.2
  - Consider the parallel electrode ionization chamber of slide I/13. As indicated on this slide, use energy conservation in the detector capacitance to obtain

$$-\frac{dU(t)}{dt} = \frac{Ne}{Cd}\left[v^- + v^+\right] \qquad -\Delta U(t_d^+) = U_\circ - U\left(t_d^+\right) = \frac{Ne}{C}$$

do not assume the drift velocity constant, but rather a function of the electric field strength (which strictly speaking is a function of time).

In practice the signal is small and the electric field can be considered constant.